Computational and Structural Biotechnology Journal 18 (2020) 3950–3958

COMPUTATIONAL AND STRUCTURAL BIOTECHNOLOGY JOURNAL

journal homepage: www.elsevier.com/locate/csbj

Permeation mechanisms through the selectivity filter and the open helix bundle crossing gate of GIRK2

Dai-Lin Li [a], Liang Hu [b], Lei Wang [a], Chin-Ling Chen [b,c,d,*]

[a] Key Laboratory of Environmental Biotechnology (XMUT), Fujian Province University, Xiamen University of Technology, Xiamen 361005, China
[b] School of Computer and Information Engineering, Xiamen University of Technology, Xiamen 361005, China
[c] School of Information Engineering, Changchun Sci-Tech University, Changchun 130600, China
[d] Department of Computer Science and Information Engineering, Chaoyang University of Technology, Taichung 41349, Taiwan

ARTICLE INFO

Article history:
Received 1 September 2020
Received in revised form 23 November 2020
Accepted 23 November 2020
Available online 02 December 2020

Keywords:
G protein-gated inwardly rectifying K^+ 2 (GIRK2), permeation mechanism
Helix bundle crossing gate
Inward rectifier potassium (Kir) channel
Molecular dynamics

ABSTRACT

G protein-gated inwardly rectifying potassium channels (GIRK) are essential for the regulation of cellular excitability, a physiological function that relies critically on the conduction of K^+ ions, which is dependent on two molecular mechanisms, namely selectivity and gating. Molecular Dynamics (MD) studies have shown that K^+ conduction remains inefficient even with open channel gates, therefore further detailed study on the permeation events is required. In this study, all-atom MD simulations were employed to investigate the permeation mechanism through the GIRK2 selectivity filter (SF) and its open helix bundle crossing (HBC) gate. Our results show that it is the SF rather than the HBC or the G-loop gate that determines the permeation efficiency upon activation of the channel. SF-permeation is accomplished by a water-K^+ coupled mechanism and the entry to the S1 coordination site is likely affected by a SF tilt. Moreover, we show that a 4-K^+ occupancy in the SF-HBC cavity is required for the permeation through an open HBC, where three K^+ ions around E152 help to abolish the unfavorable cation-dipole interactions that function as an energy barrier, while the fourth K^+ located near the HBC allows for the inward transport. These findings facilitate further understanding of the dynamic permeation mechanisms through GIRK2 and potentially provide an alternative regulatory approach for the Kir3 family given the overall high evolutionary residue conservation.

1. Introduction

G protein-gated inwardly rectifying potassium channels (GIRK or Kir3) are essential for the regulation of cellular excitability and have been reported to be involved in diverse neuronal physiological and pathophysiological processes such as analgesia [1], reward [2–7], anxiety [8], memory [9], respiration [10], seizures [11] and heart rate control [12]. Considering that these functions rely critically on the ability of the channels to conduct ions, it is important to understand the detailed permeation mechanism that contributes to ion conduction.

GIRK2 is a member of the Kir3 channel family that functions in the form of a homo-tetramer. The translocation of extracellular ions into the intracellular matrix encounters three constrictions, namely the selectivity filter (SF), the helix bundle crossing (HBC) gate, and the cytosolic G-loop gate, all of which have been identified by X-ray crystallography [13,14]. The SF is formed at the interface of four channel subunits, with each subunit contains a linearly extended backbone of highly conserved residues (T-I-G-Y-G), the carbonyl groups of which form a four-fold symmetric narrow filter. This arrangement generates four equidistant K^+ binding sites (Fig. S1a, b) [13,14]. The HBC gate that comprises a F192 side chain is located approximately 20 Å below the SF. These two constrictions are connected by a cavity. The third constriction located about 15 Å lower than the HBC gate is formed by a loop coined as the G loop that contributes to the long-pore characteristic of Kir channels (Fig. S1a) [13,14].

The SF is responsible for the accommodation of water permeation and the selection of K^+ over Na^+ and other ions. To date, two possible mechanisms of K^+ flux through SF have been proposed. In the first model, water molecules and K^+ ions have been shown to co-translocate through the SF in an alternating K^+/water/K^+/ water arrangement through the four binding sites in the SF (Fig. 1) [15,16]. In the second model, K^+ ions have been shown

* Corresponding author at: School of Computer and Information Engineering, Xiamen University of Technology, Xiamen 361005, China.
E-mail addresses: lidl@xmut.edu.cn (D.-L. Li), lhu@xmut.edu.cn (L. Hu), wangl@xmut.edu.cn (L. Wang), clc@cyut.edu.tw (C.-L. Chen).

https://doi.org/10.1016/j.csbj.2020.11.039
2001-0370/

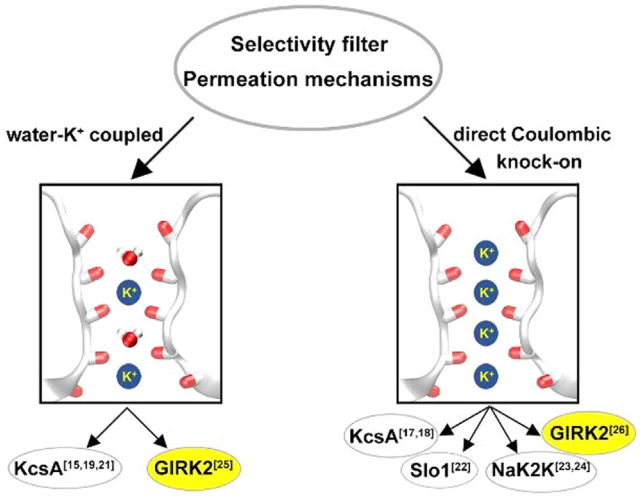

Fig. 1. Two possible permeation mechanisms through the selectivity filter of ion channels. The related channels are indicated at the bottom of each mechanism. The GIRK2 channel that is involved in both permeation mechanisms requires further clarification.

to translocate through the SF using a direct Coulombic knock-on mechanism without being accompanied by water molecules (Fig. 1) [17,18]. These two possible mechanisms have respectively been shown to be exerted by several types of K^+ channels. For instance, in the KcsA channel, the water-K^+ coupled transition states have been shown in SF permeation by Molecular Dynamics (MD) free energy simulations [19]. The water-K^+ coupled transportation in the SF of a semi-synthetic KcsA channel has been revealed using a combination of 2D IR spectra measurement, site-specific heavy isotope labeling and MD simulations [20]. In the bacterial KcsA channel, the water-K^+ coupled transport through SF has been demonstrated through its atomic-resolution crystal structure, functional characteristics and ion-binding properties [21]. However, MD simulations together with free-energy calculations have demonstrated that both rapid permeation of K^+ and ion selectivity are due to the direct knock-on of completely desolvated ions in the SF of KcsA [18]. In the SF of mammalian large conductance Ca^{2+}-activated potassium (Slo1) channel, it has been suggested that the co-transportation of water molecules with K^+ ions is not required [22]. In the NaK2K channel, single wavelength anomalous dispersion X-ray diffraction data have experimentally shown that all ion binding sites within the SF are fully occupied by K^+ ions, which in turn supports a direct Coulombic knock-on mechanism [23]. Moreover, the SF has been shown to be free of water molecules in the channel under physiological conditions, which is consistent with a direct knock-on mechanism of ion conduction [24].

Despite extensive studies on numerous types of K^+ ion channels, the SF-permeation mechanism of GIRK2 remains largely unexplored. Particularly, there is still insufficient dynamic evidence that demonstrates whether an alternating water-K^+ coupled arrangement or a direct Coulombic knock-on mechanism is the dominating SF-permeation mechanism of GIRK2. The release of GIRK2 crystal structure in 2011 [11], has facilitated a Brownian Dynamics study in 2013 to explore the conductance properties of the channel [25]. Although the mechanism of water-K^+ coupled permeation through SF has been demonstrated (Fig. 1), the outcomes may be biased as the channel is forced to open by restraints rather than regulated by intracellular modulators [25]. A very recent MD study reporting on the conduction of K^+ ions through the GIRK2 SF has demonstrated a direct knock-on mechanism through the SF via the activation of GIRK2 using the intracellular regulator phosphatidylinositol bisphosphate (PIP_2) alone (Fig. 1) [26]. However, the validity of their conclusions is being questioned by the fact that PIP_2 alone is insufficient to significantly activate GIRK2, which has been substantially tested by both electrophysiological experiments and our previous MD simulations [27,28]. Although it has been argued that PIP_2 alone is sufficient for the activation by comparing the F192 (HBC gate) Cα-Cα as well as the minimum distances in the presence/absence of the regulator, we have found this approach to be primarily structure-dependent and insufficient to draw any conclusions from [28]. In essence, if the simulations start with a HBC-closed conformation of GIRK2, PIP_2 alone is unable to activate the channel even reaching a micro-second time scale [28].

The HBC and G loop gates control K^+ ion conduction through GIRK2 channels. To our knowledge, if both the HBC and G-loop gates were to stay opened, the channel would be considered conductive for K^+ ions accordingly. Unexpectedly, our simulations have shown that K^+ ions in the SF-HBC cavity are unable to permeate the open HBC/G-loop gates of GIRK2 even with the aid of an external electric field. In other words, the cations are not able to permeate freely when both gates are open (Fig. 2), suggesting that there may be an additional requirement for the permeation in addition to the channel conductive state.

In order to clarify the mechanism of K^+ flux through the SF (Fig. 1) and to identify the requirement that allows K^+ to permeate the open HBC gate of GIRK2 (Fig. 2), all-atom MD simulations of PIP_2-, Na^+- and Gβγ subunit-activated channel were applied in this study. Our results facilitate further understanding of the dynamic permeation mechanism. In view of the high evolutionary conservation of residues involved in the permeation pathway, our data may potentially provide an alternative regulatory approach for the Kir3 family.

2. Materials and methods

2.1. Preparation of initial models for simulations

Our simulations include two major stages as shown in Fig. 3: preparation of initial models (stage 1) and all-atom MD (stage 2). In stage 1, all the preparations were done on three wild-type models. The GIRK2 crystal structure comprising the intracellular regulators, such as PIP_2, Na^+, and Gβγ retrieved from the Protein Data Bank (PDB ID: 4KFM) was taken as the initial model. The other two models were built by removing Na^+ or Gβγ respectively from the initial model. The three wild-type complexes obtained include GIRK2-PIP_2-Na^+ (GIRK2-Na^+), GIRK2-PIP_2-Gβγ (GIRK2-Gβγ) and GIRK2-PIP_2-Gβγ-Na^+ (GIRK2-Gβγ-Na^+).

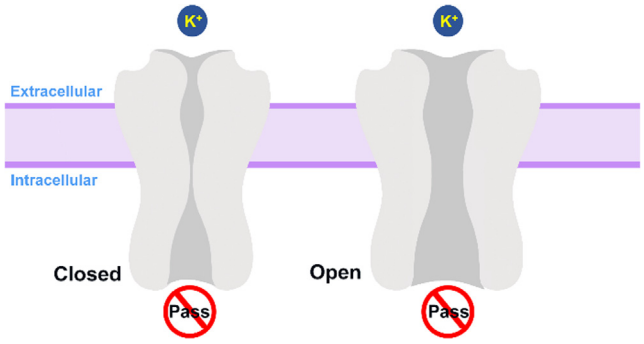

Fig. 2. K^+ ions permeating the GIRK2 channel from the extracellular to the intracellular side. K^+ ions are unable to pass through the channel in a closed conformation. Unexpectedly, K^+ ions are unable to permeate an open HBC/G-loop gates of GIRK2 even with the aid of an external electric field, suggesting there may be an additional requirement for the permeation in addition to the channel conductive state.

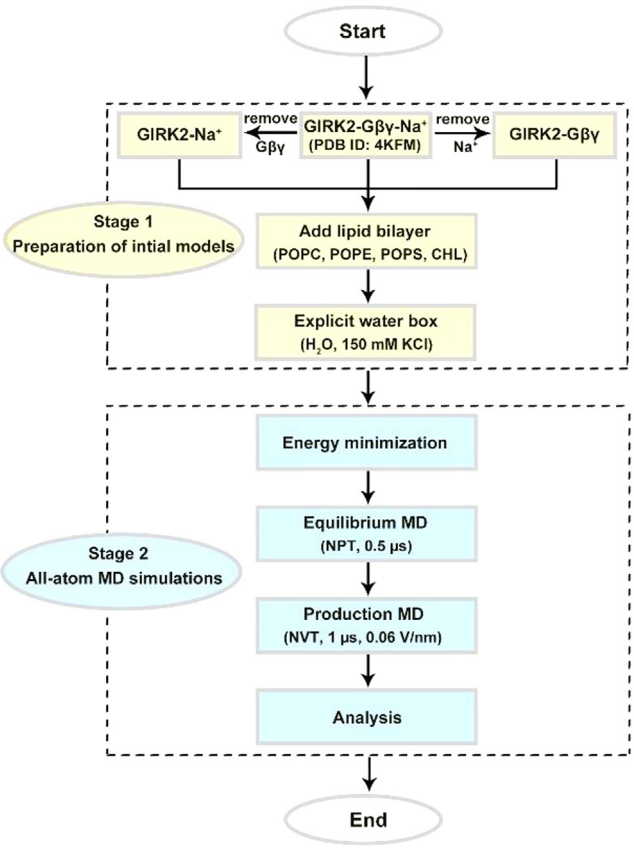

Fig. 3. Computational protocols for simulations, including two major stages colored in yellow and cyan individually. The details of each step are outlined in the Materials and Methods section. (For interpretation of the references to colour in this figure legend, the reader is referred to the web version of this article.)

All the missing heavy atoms were added based on the standard L-residue template by PyRosetta built on Python-2.7 [29]. All the hydrogen atoms were added using the H++ website server [30,31]. The protonation states of the titratable residues were determined by pKa calculations at neutral physiological conditions (pH = 7.0). The PIP_2 molecule was built by adding the missing alkyl tails in the X-ray structure (PDB ID: 4KFM). The geometry optimization and the restrained electrostatic potential charge were done by the ESP module of NWChem 6.8.1 [32]. To mimic the behavior of GIRK2 on an experimentally feasible membrane, the explicit lipid bilayer of POPC, POPE, POPS and cholesterol (CHL) with the molecular ratio of 25:5:5:1 was employed by the CHARMM-GUI Membrane Builder web server [33–36]. All the components plus 150 mM KCl were immersed into a water box ($116 \times 116 \times 150$ Å^3 for GIRK2-Na^+ and $162 \times 162 \times 170$ Å^3 for GIRK2-Gβγ and GIRK2-Gβγ-Na^+, respectively) with at least 14 Å from the protein periphery in each dimension. The simulation systems as a consequence contain 160,000 to 400,000 atoms.

2.2. All-atom microsecond-scale MD simulations

All-atom microsecond-scale MD simulations in stage 2 (Fig. 3) were done by the Amber16 software package [37]. A two-step energy minimization protocol (steepest descent and conjugate gradient algorithm) was performed by 10,000 steps each, with FF14SB [38], LIPID17 [39,40], and GAFF2 [41–43] force fields for protein, lipid membrane and PIP_2, respectively. This set of force field parameters has been shown to be capable of probing the activation and the deactivation of the GIRK2 channel reasonably, particularly the gating mechanism by the same modulators in the present study [28]. Next, heating from 0 to 300 K was achieved using the Langevin thermostat algorithm [44], with a time step of 0.5-femtosecond (fs) to avert internal disturbance. In the heating stage, the protein and lipid bilayer were fixed to remove any potential steric clashes from K^+ or Cl^- ions, and water molecules. At the target temperature, the position restraints were gradually lowered in 10 steps from 10 to 0.1 kcal/mol·Å^2 in 20 ns (ns).

The equilibrium MD simulations were conducted at constant temperature and pressure ensemble (NPT) for 0.5 microseconds (μs), followed by production jobs at constant temperature and volume ensemble (NVT) for 1 μs. To accelerate the permeation events, an external voltage at 0.06 V/nm from the extra- to intracellular side was applied as outlined in previous studies [28,45,46], under which the secondary structure of all subunits of GIRK2 was well maintained. Accordingly, transmembrane voltage was estimated to be around −200 mV based on the transmembrane thickness of around 32 Å. In the equilibrium/production stage, long-range electrostatics were calculated using the particle mesh Ewald (PME) method with a 10 Å cutoff, considering that the computational expense on more than 400,000 atoms was in a time scale of μs. To further accelerate the MD simulations, a 4-fs time step by the hydrogen mass repartition algorithm was employed for the solutes [47]. As for the solvent molecules, the SHAKE algorithm was applied [48,49]. The size and permeation events of each simulated system were summarized in Table S1.

All the analyses were done on the GIRK2-Gβγ-Na^+ model with an external electric field unless otherwise mentioned. Structural geometry calculation and statistical analyses were done using our private code executed in MD Analysis 0.18 [50,51]. Water molecules within 3 Å of the given average distance of a permeating K^+ ion were identified for hydration. To explore the hydrated state of K^+ in permeation, the number of water molecules in the hydration shell right before and after the permeant movement was labeled. Permeant movement means complete permeation of a K^+ ion in the current snapshot through a constriction (SF, HBC, or G loop) in the next snapshot. To locate the factors that affect the recognition of S1 by extracellular K^+, a SF tilt angle is defined as illustrated in Fig. S1, where vertical Z-axis is the unit representation of 'along the channel pathway'; angle is determined by the Cα atom geometry center of T100, G104 and the Z-axis. To identify the energetic barrier contributors for the process of K^+ permeation through the HBC gate, pairwise non-bonded interactions (Van der Waals and electrostatic interactions) were calculated by the NAMD energy plugin for VMD 1.9.3 with default parameters [52]. VMD was also used for cartoon representation rendering [52]. Sequence conservation analyses on GIRK2 were performed to evaluate the evolution variability of functional residues using the ConSurf server [53–55]. All calculations were conducted on servers equipped with NVIDIA GeForce GTX-1080 graphical cards.

3. Results and discussion

3.1. SF determines the permeation efficiency of K^+ ions

3.1.1. Hydration state of K^+ through constrictions of the permeation pathway

As discussed above, GIRK2 viewed from the extra- to the intracellular side comprises three constrictions along the channel pathway, namely SF, HBC gate and G-loop gate. As the SF plays a role in the selection of K^+/water over Na^+ and other ions, the channel is generally considered to be K^+-permeable when both gates (HBC and G-loop gate) are opened. Taking the diameter of hydrated K^+ ions into consideration, the constriction gates with a size wider than a minimum distance of 8 Å seem necessary for the conduc-

tion. For example, among the available X-ray crystal structures of GIRK2 at atomic resolution, the only "open" conformation (PDB ID: 3SYQ) captures the HBC gate at around 10.02 Å [13,14,28]. Based on our previously published data, a much narrower gate at around 5.69 Å, has been found to fulfill the requirement for K^+ transport [28].

To illustrate the flux of K^+ through such narrow gates, we first explored the hydration state of permeating K^+ ions. The GIRK2-Gβγ-Na^+ system with the highest number of permeation events was selected for hydration analysis. Moreover, the trajectory after 0.2 μs at the production stage was taken into consideration since the equilibrium state was reached after 0.2 μs (Fig. S2). Fig. 4 shows the number of water molecules in the hydration shell of K^+ ions right before and after passing through each constriction point, including SF, HBC and G-loop gate. The number of water molecules was found to be less than 2 as K^+ ions passed through the SF (Fig. 4), indicating a dehydrated inflow. In contrast, up to 7 water molecules were revealed to be typical for permeation through both the HBC and G-loop gates (Fig. 4). Taken together, our MD results showed that, whilst K^+ ions are dehydrated when passing through the SF; they are partially hydrated when passing through the HBC and G-loop gates. These findings are consistent with a prior simulation study of a GIRK1 chimera [46]. Hence, partial hydration during gate penetration is likely to account for a smaller gate (5.69 Å instead of 8 Å or greater was required).

3.1.2. SF determines the permeation efficiency

GIRK2-Gβγ-Na^+ complex has been reported to be more K^+-conductive than GIRK2-Gβγ or GIRK2-Na^+ due to a synergism of the intracellular regulators Gβγ and Na^+ working together to produce a greater level of activity [56]. In agreement with the experimental results, data from our MD simulations showed a 5-fold increase of permeation events for GIRK2-Gβγ-Na^+ when compared to the activity of GIRK2-Gβγ (Table S1). Accordingly, it is intriguing to note that similar channel open probabilities (the fraction of time over the simulation when both gates were in a permissive state with a minimal distance of 5.69 Å for ion flow) of 61.3% vs 68.5%

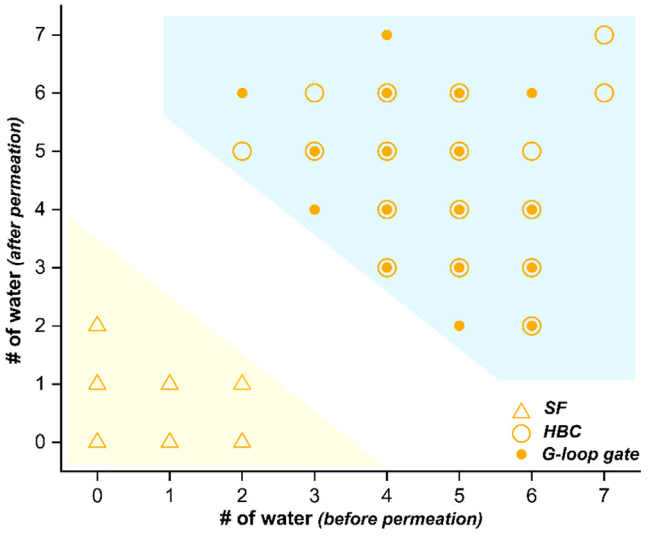

Fig. 4. The number of water molecules for hydration right before and after the permeant movement of K^+ ions through the constrictions (SF, HBC and G-loop gate) of the GIRK2-Gβγ-Na^+ system. Different hydration states are distinguished by yellow and blue colors. The incoming K^+ ions are dehydrated through SF but partially hydrated through HBC and G-loop gate. (For interpretation of the references to colour in this figure legend, the reader is referred to the web version of this article.)

in Gβγ-containing models lead to such a remarkable current difference with the addition of Na^+.

To identify the determinants for K^+ ion flow, the duration of time spent through each constriction (t_{SF}, t_{HBC}, $t_{G\ loop}$) was compared in three wild-type systems (GIRK2-Gβγ, GIRK2-Na^+, and GIRK2-Gβγ-Na^+). As shown in Fig. 5, the time required for permeation through SF was at least 4-times longer compared to that needed for passing through HBC or G-loop gates in each system, suggesting that the permeation efficiency of K^+ ions is determined by SF. GIRK2 in an activation state has a lower t_{SF} and hence a greater level of permeation. This observation is likely to account for the dramatic difference in the K^+ currents of GIRK2-Gβγ and GIRK2-Gβγ-Na^+ despite the similar open probabilities of the constriction gates.

3.2. Water and K^+ ions co-translocate through the SF

3.2.1. Water and K^+ ions co-translocate through the SF

As mentioned earlier, two distinct permeation mechanisms have been proposed to explain the flux of K^+ ions through the SF. In this study, water and K^+ ions were found to co-translocate through the SF of GIRK2 in a water-K^+ coupled manner (Fig. 6a). To better understand the permeation mechanism, the positions of water and K^+ ions of each snapshot in the production stage were firstly analyzed, and the time distributions of each major conduction step were determined. As shown in Fig. 6a, the S2/S4 K^+-bound configuration separated by water molecules (at the S1/S3 sites) took the highest proportion of the simulation time (up to 63.5%), and is believed to dominate transport through the SF. The stabilized S2/S4 occupancy configuration has also been identified in other K^+ ion permeable channels. For instance, in the KirBac1.1 channel, the minimum free energy surface has been found to be due to a configuration of K^+ ions in the S2/S4 arrangement [57]. Furthermore, the crystal structures of KcsA mutants (G77A and G77C) atomic resolution have been found to be stabilized in the S2/S4 K^+-bound configuration [21]. Overall, results from our simulations are consistent with the simulation and experimental data obtained from other K^+ ion channels.

Besides the S2/S4 K^+-bound configuration that indicated a water-K^+ coupled permeation mechanism through the SF, three additional paths were observed to mediate ions transport (Fig. 6a). In path I, an incoming extracellular K^+ at the SF was found to occupy the binding position S2 without stopping at S1. As the ions at S2 and S4 moved inwardly by two positions, the flow of the K^+ from S4 to cavity was accomplished. In path II, a K^+ was observed to firstly enter S1 before moving towards S2 to form an S2/S3/S4 occupancy. The K^+ at S4 was then repelled to enter the cavity followed by the flux of K^+ from S3 to S4. In path III, an S1/S3 to S2/S4 water-K^+ coupled arrangement was observed. It should be noted that there was an additional 7% of simulation time in the S1/S4 configuration in addition to the three paths. This configuration was found to arise only from the dynamic translocation of S2 (S2/S4) to S1(S1/S4) and thus it was not listed as a fourth path. In order to further explore the factors that influence the water-K^+ coupled permeation mechanism, its entry into SF was investigated.

3.2.2. SF tilt affects the recognition of S1 by extracellular K^+

The S2/S4 K^+-bound configuration represents the state with the highest level of occupancy in our MD trajectory. As the only way of translocation to S2, the recognition of S1 is the first and key step to start the passage through the SF. In fact, the loss of K^+ binding to the S1 site has been implicated in the SF inactivation of K_v channels [58], hERG channels [59] and TREK-2 K_{2P} channels [60]. Thus, it is necessary to investigate the recognition of S1 by extracellular K^+ ions in order to thoroughly assess the permeation mechanism.

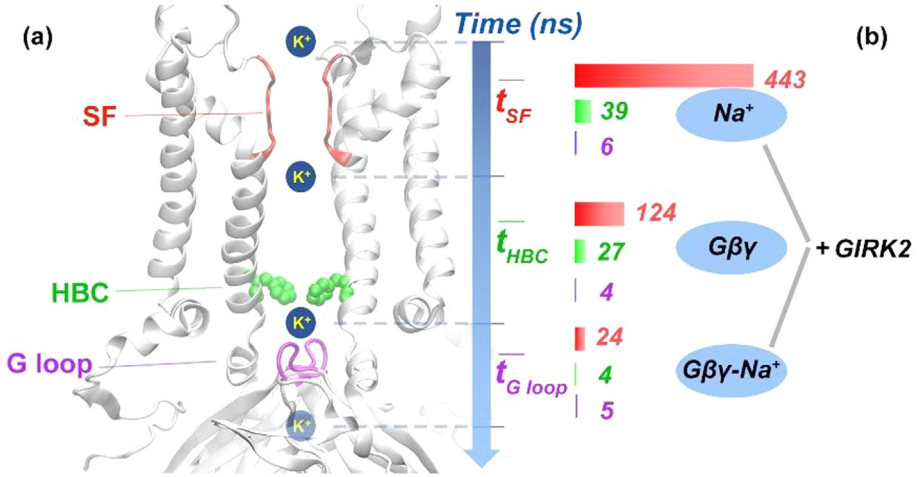

Fig. 5. (a) Secondary structure representation of two opposite subunits (chains) of GIRK2 channel with the three constrictions highlighted in red, green and purple, respectively; (b) average time duration (ns) required by K^+ ions for permeation through SF, HBC and G-loop gate of the three wild-type systems. SF is the determinant for permeation efficiency since the t_{SF} is at least 4-fold of t_{HBC} and $t_{G\ loop}$ in each system. (For interpretation of the references to colour in this figure legend, the reader is referred to the web version of this article.)

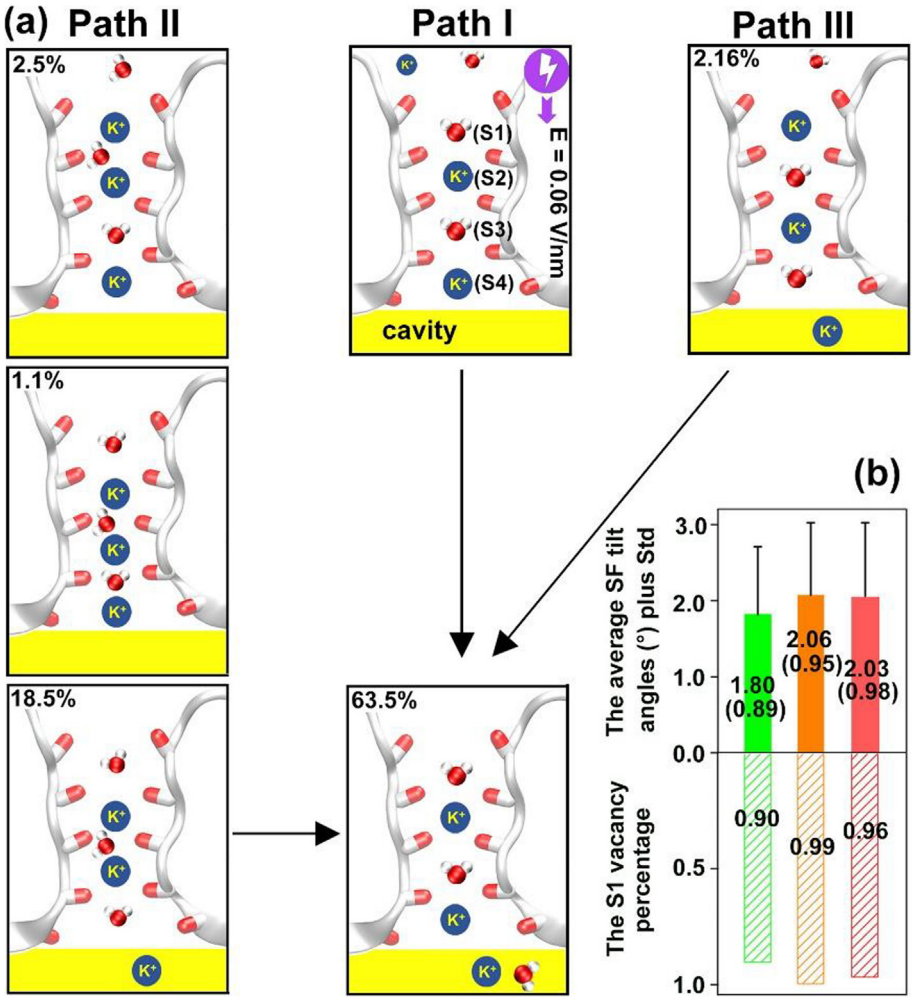

Fig. 6. (a) Permeation mechanism through the SF of GIRK2. Time distribution (%) of major steps and the coordination binding sites (S1-S4) are labeled. There are three translocation paths under an external voltage of 0.06 V/nm (purple arrow is shown in Path I only). The S2/S4 K^+-bound configuration separated by water molecules takes the most simulation time, which indicates that water and K^+ ions co-translocate through SF in a water-K^+ coupled manner. (b) The average SF tilt angles and the standard deviations of GIRK2-Gβγ-Na^+ (green), GIRK2-Gβγ (orange) and GIRK2-Na^+ (red). The corresponding S1 vacancy percentage is listed below. GIRK2-Gβγ-Na^+ shows the lowest degree of average tilt angle and fluctuation but exhibits the highest S1 occupancy percentage as a result. (For interpretation of the references to colour in this figure legend, the reader is referred to the web version of this article.)

With the aid of an extra- to intracellular directed external electric field (Fig. 6a), K^+ ions prefer moving into the cell directly. If a tilt were to occur in the SF (Fig. S1a), the entrance to SF would be decreased accordingly (Fig. S3), which may cause difficulties for extracellular K^+ to recognize the S1 site. Amongst all the simulation systems, GIRK2-Gβγ-Na^+ shows the lowest degree of average tilt angle and fluctuation compared to those of GIRK2-$Na^+$and GIRK2-Gβγ, and exhibits the highest S1 occupancy percentage at 3- to 14-fold as a consequence (Fig. 6b). These data suggest that a less degree of SF tilt results in a longer occupancy of S1. Thus, the SF tilt of GIRK2 is likely to affect the entrance of extracellular K^+ ions to the channel. Recently, a SSNMR study of KirBac1.1 has indicated that, the S4 binding site is expected to be involved in the conductive state of SF, and that deformation at S4 might refer to a nonconductive state [61]. Due to the homology between KirBac1.1 and Kir3.2, how the S4 binding site relates to the permeation efficiency through SF remains to be further clarified.

3.3. A 4-K^+ occupancy in cavity is required for permeation through an opened HBC gate

3.3.1. A 4-K^+ occupancy for permeation through an opened HBC

In general, the GIRK2 channel with both constriction gates opened is thought to be conductive for K^+ ions based on electrophysiological experiments. However, in this study, there is a significant period of simulation time with no K^+ ions flux detected even though the HBC and G-loop gates are kept opened with a probability of up to 81.4% and 79.6%, respectively in the GIRK2-Gβγ-Na^+ model, additional factors are required for the permeation at a given electrochemical driving force. Our simulation trajectories of all the models clearly showed that permeation through an activated GIRK2 only occurred when the number of accumulated K^+ ions in cavity is up to 4 (Fig. 7). When the number is less than 4, almost all attempts of K^+ passing through an opened HBC gate failed regardless of the time taken.

In order to prepare for permeation, K^+ ions in the cavity are firstly required to relocate to the region near HBC. Unfortunately, such an inward movement is likely to be limited by the outward electrostatic attractions induced by the negatively charged carboxyl group of E152 (Fig. 8a, S1a). Under a 3-K^+ pattern, K^+ ions prefer E152 (69.8%) to the HBC gate (29.8%), which in turn hinders the preparation for permeation; in contrast, HBC is favored (50.2%) under a 4-K^+ occupancy (Fig. 8). Obviously, the 4-K^+ pattern is

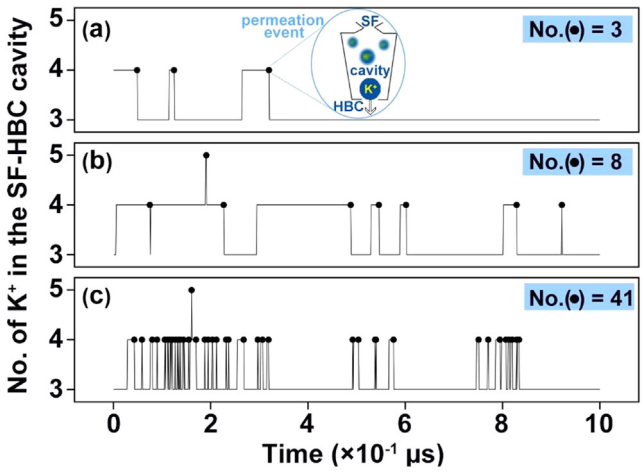

Fig. 7. Number of K^+ ions in the SF-HBC cavity vs simulation time of (a) GIRK2-Na^+, (b) GIRK2-Gβγ and (c) GIRK2-Gβγ-Na^+ systems. Each black dot represents a permeation event through the HBC gate. The K^+ permeation through an open HBC gate is only successful when the number of accumulated ions in cavity is 4 or more.

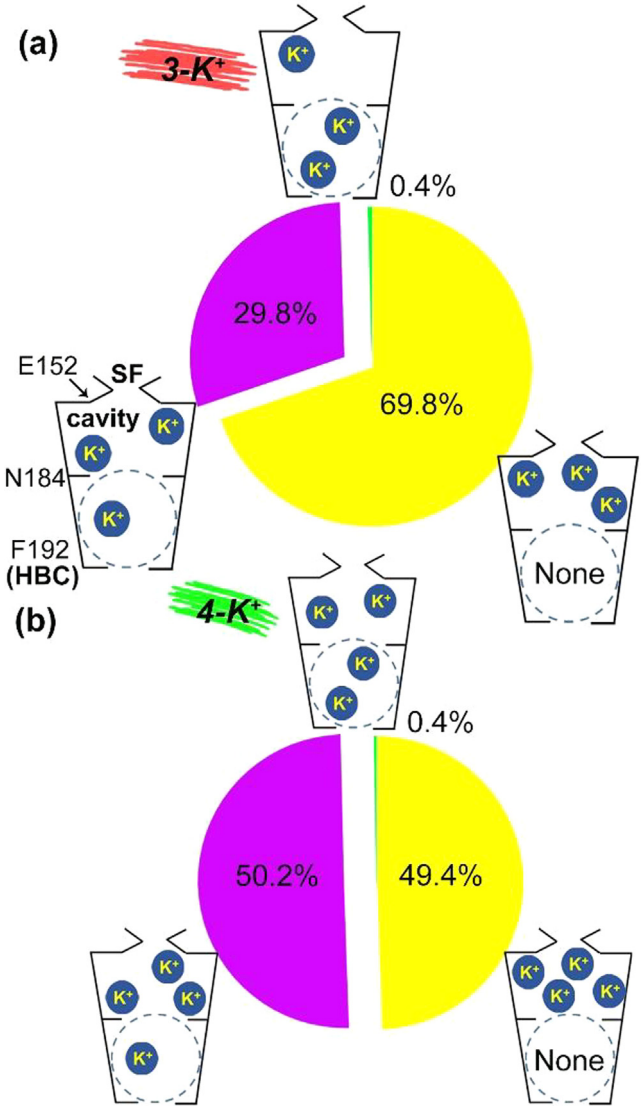

Fig. 8. Time distribution (%) of K^+ ions in SF-HBC cavity for (a) 3-K^+ and (b) 4-K^+ occupancy. A total of three distributed locations of K^+ are involved in the flux through HBC in each occupancy, and the time percentage of each location is indicated in purple, green, and yellow. With N184 as the middle boundary, the cavity can be divided into two regions, where the upper region is near E152 and the lower region is next to HBC. In order to prepare for the inward permeation, K^+ ions in the cavity need to firstly move to the region near HBC (circled by blue dash lines). Under a 3-K^+ pattern, K^+ ions prefer E152 (69.8%) to the HBC gate (29.8%), which in turn hinders the preparation for permeation. In contrast, HBC is the favorite (50.2%) under 4-K^+, which facilitates the preparation for permeation. Water molecules of hydration are removed for clarity. (For interpretation of the references to colour in this figure legend, the reader is referred to the web version of this article.)

easier than the 3-K^+ pattern to prepare for permeation through the HBC gate in light of the location distributions. These findings are further supported and complemented by a 10 μs MD simulation on the GIRK2 mutant R201A (unpublished data), where amongst 46 permeation events, 35 events were found to occur under the 4-K^+ pattern and 11 events were observed to occur under the 3-K^+ pattern. This indicated that the 4-K^+ pattern dominates the K^+ translocation through the HBC gate.

3.3.2. A 4-K^+ pattern decreases the permeation energy barrier by competitive attractions to N184

To further identify the permeation mechanism through the open HBC of GIRK2, K^+(HBC)-residue(cavity) pair-wise non-

bonded interactions were estimated. Since non-polarizable force field was employed, the non-bonded interactions were only used to identify the residues in the SF-HBC cavity with a higher level of contribution towards the permeation barrier. Fig. 9a shows that

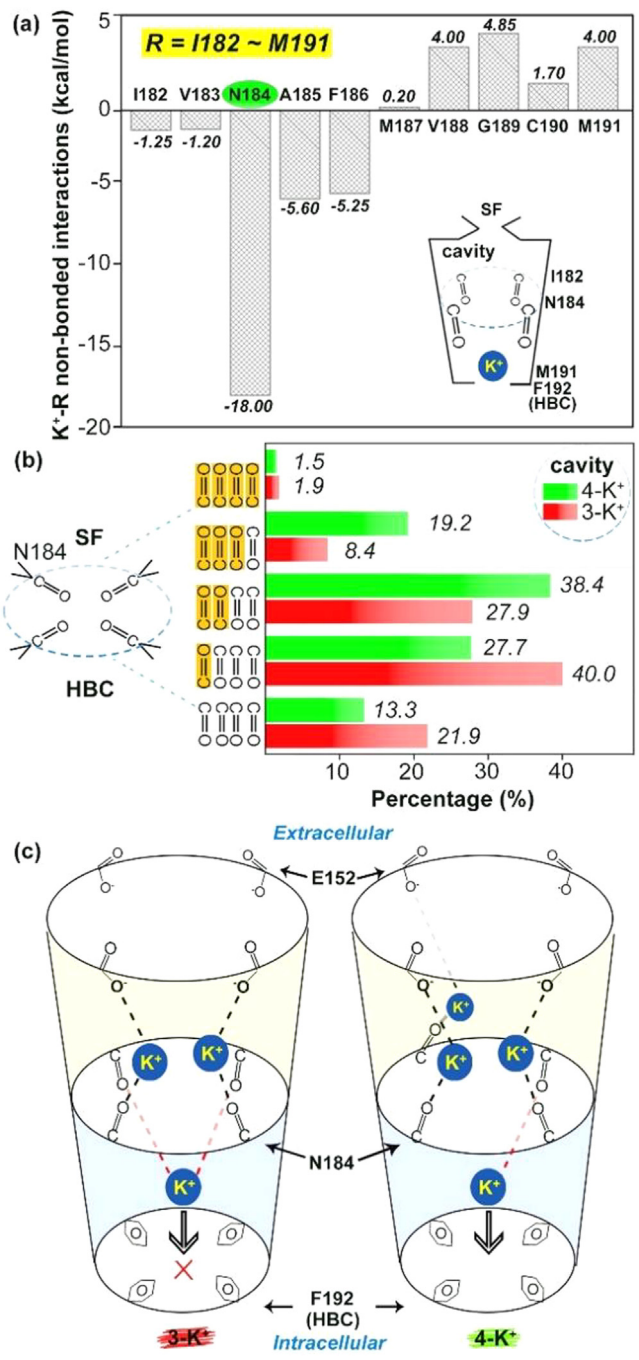

Fig. 9. (a) Pair-wise non-bonded interactions (kcal/mol) of K^+(HBC)-residue(cavity) while four subunits of N184 carbonyl groups have unfavorable conformations for permeation through HBC. (b) Time distribution of five orientation combinations of N184 carbonyl groups under 4-K^+ and 3-K^+ patterns, with the favorable conformation highlighted in yellow. (c) Permeation mechanism of K^+ through opened HBC gate. Permeation is only allowed through the 4-K^+ pattern due to less unfavorable cation-dipole interactions (a red line on the right). Three K^+ in the upper cavity (yellow region) are attracted by E152 to induce the formation of favorable upward orientation of N184 carbonyl groups through direct interactions. As a result, outward pulling force for permeation is decreased and the fourth K^+(HBC) is allowed for inward transport. Water molecules of hydration are omitted for clarity. (For interpretation of the references to colour in this figure legend, the reader is referred to the web version of this article.)

N184 has the highest level of contribution towards the permeation barrier of up to −18 kcal/mol when the carbonyl groups of four constituent subunits adopt an inward conformation. Due to the presence of a carbonyl group inside the side chain, the interactions between K^+(HBC) and N184 are inferred to arise in the form of cation-dipole. Although the presence of negative energy indicates that K^+(HBC) is attracted by N184, this outward pulling force is considered unfavorable for inward permeation.

To test the role of N184 in preventing the ion flow through an open HBC, the conservation analysis of functional residues was firstly performed. Although residue184 exhibited variability in position conversation across the Kir family (Fig. S4), N184 has been proven experimentally to play a role as a structural element for K^+ transport through GIRK2. Introduction of a negative charge at N184 has been shown to dramatically increase the selectivity for K^+ over Na^+, and improve the channel inward rectification [62].

Secondly, the time distribution was analyzed based on the orientation of the carbonyl group in the four subunits. As shown in Fig. 9b, under a 3-K^+ pattern, the N184 of one or two subunits holds a carbonyl group in a favorable conformation for up to 67.9% of the total simulation time. No permeation events were observed in this conformation, suggesting that three or four subunits of N184 in a favorable orientation may be required. Although a considerable 10.3% (8.4%+1.9%) of the favorable orientation of the carbonyl groups was located under a 3-K^+ pattern (Fig. 9b), the level of K^+ distribution around the HBC was 29.8% only (Fig. 8b). A total of only 3.1% (10.3% × 29.8%) permeant probability that satisfied both the energy and the location factors was obtained. In contrast, the percentages of both factors in a 4-K^+ pattern were significantly increased to 20.7% and 50.2%, respectively (Fig. 9b and 8a) with a simultaneous fold gain of up to 3.5-fold. This is in agreement with the permeant probability of our ongoing study on the GIRK2 mutant R201A, in which the permeation events of a 4-K^+ pattern compared to those of a 3-K^+ pattern were found to differ by approximately 3.2-fold.

The abolishment of the unfavorable cation-dipole interactions between K^+(HBC) and N184 has been demonstrated above to facilitate the ion passage. However, how the interactions were abolished remains unclear. With N184 as a middle boundary, the cavity can be divided into two regions where the upper region is located near E152 and the lower region is located next to the HBC. As shown in Fig. 9c, movement of K^+ ions at the upper part is likely to cause abolishment of the unfavorable K^+(HBC)-N184 interactions, since the K^+(E152) is able to induce cation-dipole with N184 in a similar way to that with K^+ (HBC). In other words, the energy barrier for permeation through the HBC is determined by the competitive cation-dipole attractions induced by K^+(HBC) and K^+(E152) ions. If the number of K^+(E152) ions is insufficient to truncate 75% of the unfavorable K^+(HBC)-N184 interactions, the ion flow through an open HBC is difficult to occur. As shown in Fig. 9c, 50% of the K^+(HBC)-N184 interactions has been ruined under the 3-K^+ pattern (two red lines on the left), resulting in no permeation events; however, 75% of K^+(HBC)-N184 interactions abolished under the 4-K^+ pattern (one red line on the right) resulted in permeation events.

Finally, we addressed why the 4-K^+ pattern in cavity benefits both the distributions of K^+(HBC) and the favorable conformation of the N184 carbonyl group. On one hand, the negative charge of E152 (four subunits) is prone to restraining a positive K^+ around individually when three cations co-exist in the cavity. As clearly shown in Fig. 8, three K^+ ions prefer the upper region of cavity, occupying it 69.8% of the simulation time. As a fourth K^+ comes in, the enhanced positive repulsion makes it less stable to accommodate four cations around E152; consequently, one K^+ is pushed into the region of HBC (Fig. 8). Based on the conservation analysis, residue 152 (GIRK2-based number) shows a higher level of evolu-

tionary conservation across ten Kir family members (Fig. S4). However, this value is expected to be higher in the Kir3 family since residue 152 has always been a glutamic acid residue. These results may imply a significant role of negative charge on residue 152.

On the other hand, the favorable conformation of the N184 carbonyl group is achieved through the induction from K^+ around E152 (Fig. 9c), where the number of K^+(E152) becomes a key factor. Under a 4-K^+ pattern, one cation has to stay around HBC due to the positive repulsion as mentioned above, which makes it difficult for a second cation to get in close proximity. This results in the creation of ideal ion locations for permeation, where three K^+(E152) help to abolish the unfavorable cation-dipole interactions, while K^+(HBC) is allowed to go through the HBC gate inwardly (Fig. 9c).

4. Conclusions

All-atom MD was employed to investigate the K^+ ions permeation mechanisms through the SF and the open HBC gate of GIRK2 channel. The SF, instead of the HBC or G-loop gate determines the permeation efficiency when the channel is activated. SF-permeation is accomplished by the water-K^+ coupled mechanism and the SF tilt is likely to affect the recognition of S1 binding site by extracellular K^+ ions. Moreover, the 4-K^+ occupancy in the SF-HBC cavity is required for the permeation through an open HBC; whilst three K^+(E152) ions help to abolish the unfavorable cation-dipole interactions that function as the energy barrier, the fourth K^+(HBC) is allowed for the inward transport. These findings may facilitate in clarifying the controversy on the ion flux through SF and in elucidating the requirement for the permeation through an open HBC gate. Our data may also potentially provide an alternative approach in the regulation of Kir3 family due to the high level of residue conservation in evolution. Given the present findings, an outward permeation mechanism requires further studies. Since the 4-K^+ occupancy functions as an additional requirement for the inward permeation, whether it works well for the outward transport of ions remains unclear. Taken together, the bidirectional outcomes will provide an overall and coherent view on the permeation mechanism of GIRK channels.

CRediT authorship contribution statement

Dai-Lin Li: Conceptualization, Methodology, Data curation, Writing - original draft, Visualization, Project administration, Funding acquisition. **Liang Hu:** Software, Validation. **Lei Wang:** Investigation. **Chin-Ling Chen:** Writing - review & editing, Supervision.

Declaration of Competing Interest

The authors declare that they have no known competing financial interests or personal relationships that could have appeared to influence the work reported in this paper.

Acknowledgements

We thank the Engineering Research Center for Medical Data Mining and Application of Fujian Province (XMUT) for the GPU-based calculation platforms. We would like to express our gratitude to EditSprings (https://www.editsprings.com/) for the expert linguistic services provided. This research was funded by the Natural Science Foundation of Fujian province (Grant No. 2020J01259) and the Xiamen University of Technology (Grant No. E201300100 and XPDKT19027).

Appendix A. Supplementary data

Supplementary data to this article can be found online at https://doi.org/10.1016/j.csbj.2020.11.039.

References

[1] Tsantoulas C, McMahon SB. Opening paths to novel analgesics: the role of potassium channels in chronic pain. Trends Neurosci 2014;37:146–58.
[2] Munoz MB, Padgett CL, Rifkin R, Terunuma M, Wickman K, Contet C, et al. A role for the GIRK3 subunit in methamphetamine-induced attenuation of GABAB receptor-activated GIRK currents in VTA dopamine neurons. J Neurosci 2016;36:3106–14.
[3] Herman MA, Sidhu H, Stouffer DG, Kreifeldt M, Le D, Cates-Gatto C, et al. GIRK3 gates activation of the mesolimbic dopaminergic pathway by ethanol. Proc Natl Acad Sci U S A 2015;112:7091–6.
[4] Lomazzi M, Slesinger PA, Luscher C. Addictive drugs modulate GIRK-channel signaling by regulating RGS proteins. Trends Pharmacol Sci 2008;29:544–9.
[5] Munoz MB, Slesinger PA. Sorting nexin 27 regulation of G protein-gated inwardly rectifying K(+) channels attenuates in vivo cocaine response. Neuron 2014;82:659–69.
[6] Kotecki L, Hearing M, McCall NM, Marron Fernandez de Velasco E, Pravetoni M, Arora D, et al. GIRK channels modulate opioid-induced motor activity in a cell type- and subunit-dependent manner. J Neurosci 2015;35:7131–42.
[7] Pravetoni M, Wickman K. Behavioral characterization of mice lacking GIRK/Kir3 channel subunits. Genes Brain Behav 2008;7:523–31.
[8] Wydeven N, Marron Fernandez de Velasco E, Du Y, Benneyworth MA, Hearing MC, Fischer RA, et al. Mechanisms underlying the activation of G-protein-gated inwardly rectifying K+ (GIRK) channels by the novel anxiolytic drug, ML297. Proc Natl Acad Sci U S A 2014;111:10755–60.
[9] Ostrovskaya O, Xie K, Masuho I, Fajardo-Serrano A, Lujan R, Wickman K, et al. RGS7/Gbeta5/R7BP complex regulates synaptic plasticity and memory by modulating hippocampal GABABR-GIRK signaling. Elife 2014;3:e02053.
[10] Montandon G, Ren J, Victoria NC, Liu H, Wickman K, Greer JJ, et al. G-protein-gated inwardly rectifying potassium channels modulate respiratory depression by opioids. Anesthesiology 2016;124:641–50.
[11] Kaufmann K, Romaine I, Days E, Pascual C, Malik A, Yang L, et al. ML297 (VU0456810), the first potent and selective activator of the GIRK potassium channel, displays antiepileptic properties in mice. ACS Chem Neurosci 2013;4:1278–86.
[12] Lee SW, Anderson A, Guzman PA, Nakano A, Tolkacheva EG, Wickman K. Atrial GIRK channels mediate the effects of vagus nerve stimulation on heart rate dynamics and arrhythmogenesis. Front Physiol 2018;9:943.
[13] Whorton MR, MacKinnon R. Crystal structure of the mammalian GIRK2 K+ channel and gating regulation by G proteins, PIP2, and sodium. Cell 2011;147:199–208.
[14] Whorton MR, MacKinnon R. X-ray structure of the mammalian GIRK2-betagamma G-protein complex. Nature 2013;498:190–7.
[15] Zhou Y, Morais-Cabral JH, Kaufman A, MacKinnon R. Chemistry of ion coordination and hydration revealed by a K+ channel-Fab complex at 2.0 A resolution. Nature 2001;414:43–8.
[16] Zhou Y, MacKinnon R. The occupancy of ions in the K+ selectivity filter: charge balance and coupling of ion binding to a protein conformational change underlie high conduction rates. J Mol Biol 2003;333:965–75.
[17] Köpfer DA, Song C, Gruene T, Sheldrick GM, Zachariae U, de Groot BL. Ion permeation in K(+) channels occurs by direct Coulomb knock-on. Science 2014;346:352–5.
[18] Kopec W, Köpfer DA, Vickery ON, Bondarenko AS, Jansen TLC, de Groot BL, et al. Direct knock-on of desolvated ions governs strict ion selectivity in K(+) channels. Nat Chem 2018;10:813–20.
[19] Berneche S, Roux B. Energetics of ion conduction through the K+ channel. Nature 2001;414:73–7.
[20] Kratochvil HT, Carr JK, Matulef K, Annen AW, Li H, Maj M, et al. Instantaneous ion configurations in the K+ ion channel selectivity filter revealed by 2D IR spectroscopy. Science 2016;353:1040–4.
[21] Tilegenova C, Cortes DM, Jahovic N, Hardy E, Hariharan P, Guan L, et al. Structure, function, and ion-binding properties of a K(+) channel stabilized in the 2,4-ion-bound configuration. Proc Natl Acad Sci U S A 2019;116:16829–34.
[22] Guo J, Tan Z, Ji Y. Permeation mechanism of potassium ions through the large conductance Ca(2+)-activated potassium channel. ACS Chem Neurosci 2019;10:3601–10.
[23] Langan PS, Vandavasi VG, Weiss KL, Afonine PV, El Omari K, Duman R, et al. Anomalous X-ray diffraction studies of ion transport in K(+) channels. Nat Commun 2018;9:4540.
[24] Oster C, Hendriks K, Kopec W, Chevelkov V, Shi C, Michl D, et al. The conduction pathway of potassium channels is water free under physiological conditions. Sci Adv 2019;5:eaaw6756.
[25] Hilder TA, Chung SH. Conductance properties of the inwardly rectifying channel, Kir3.2: molecular and Brownian dynamics study. Biochim Biophys Acta 1828 2013:471–8.
[26] Bernsteiner H, Zangerl-Plessl EM, Chen X, Stary-Weinzinger A. Conduction through a narrow inward-rectifier K(+) channel pore. J Gen Physiol 2019;151:1231–46.

[27] Sui JL, Petit-Jacques J, Logothetis DE. Activation of the atrial KACh channel by the betagamma subunits of G proteins or intracellular Na+ ions depends on the presence of phosphatidylinositol phosphates. Proc Natl Acad Sci U S A 1998;95:1307–12.
[28] Li D, Jin T, Gazgalis D, Cui M, Logothetis DE. On the mechanism of GIRK2 channel gating by phosphatidylinositol bisphosphate, sodium, and the Gbetagamma dimer. J Biol Chem 2019;294:18934–48.
[29] Chaudhury S, Lyskov S, Gray JJ. PyRosetta: a script-based interface for implementing molecular modeling algorithms using Rosetta. Bioinformatics 2010;26:689–91.
[30] Anandakrishnan R, Aguilar B, Onufriev AV. H++ 3.0: automating pK prediction and the preparation of biomolecular structures for atomistic molecular modeling and simulations. Nucleic Acids Res 2012;40:W537–541.
[31] Myers J, Grothaus G, Narayanan S, Onufriev A. A simple clustering algorithm can be accurate enough for use in calculations of pKs in macromolecules. Proteins 2006;63:928–38.
[32] Valiev M, Bylaska EJ, Govind N, Kowalski K, Straatsma TP, van Dam HJJ, et al. NWChem: a comprehensive and scalable open-source solution for large scale molecular simulations. Comput Phys Commun 2010;181:1477–660.
[33] Jo S, Kim T, Iyer VG, Im W. CHARMM-GUI: a web-based graphical user interface for CHARMM. J Comput Chem 2008;29:1859–65.
[34] Wu EL, Cheng X, Jo S, Rui H, Song KC, Davila-Contreras EM, et al. CHARMM-GUI Membrane Builder toward realistic biological membrane simulations. J Comput Chem 2014;35:1997–2004.
[35] Jo S, Lim JB, Klauda JB, Im W. CHARMM-GUI Membrane Builder for mixed bilayers and its application to yeast membranes. Biophys J 2009;97:50–8.
[36] Jo S, Kim T, Im W. Automated builder and database of protein/membrane complexes for molecular dynamics simulations. PLoS ONE 2007;2.
[37] Case DA, Betz RM, Cerutti DS, Cheatham, III TE, Darden TA, Duke RE, Giese TJ, Gohlke H, Goetz AW, Homeyer N, Izadi S, Janowski P, Kaus J, Kovalenko A, Lee TS, LeGrand S, Li P, Lin C, Luchko T, Luo R, Madej B, Mermelstein D, Merz KM, Monard G, Nguyen H, Nguyen HT, Omelyan I, Onufriev A, Roe DR, Roitberg A, Sagui C, Simmerling CL, Botello-Smith WM, Swails J, Walker RC, Wang J, Wolf RM, Wu X, Xiao L, Kollman PA. 2016, AMBER 2016, University of California, San Francisco.
[38] Maier JA, Martinez C, Kasavajhala K, Wickstrom L, Hauser KE, Simmerling C. ff14SB: improving the accuracy of protein side chain and backbone parameters from ff99SB. J Chem Theory Comput 2015;11:3696–713.
[39] Skjevik AA, Madej BD, Walker RC, Teigen K. LIPID11: a modular framework for lipid simulations using amber. J Phys Chem B 2012;116:11124–36.
[40] Dickson CJ, Madej BD, Skjevik AA, Betz RM, Teigen K, Gould IR, et al. Lipid14: the amber lipid force field. J Chem Theory Comput 2014;10:865–79.
[41] Wang J, Wolf RM, Caldwell JW, Kollman PA, Case DA. Development and testing of a general amber force field. J Comput Chem 2004;25:1157–74.
[42] Wang J, Tingjun H. Application of molecular dynamics simulations in molecular property prediction I: density and heat of vaporization. J Chem Theory Comput 2011;7:2151–65.
[43] Mobley DL, Bayly CI, Cooper MD, Shirts MR, Dill KA. Small molecule hydration free energies in explicit solvent: An extensive test of fixed-charge atomistic simulations. J Chem Theory Comput 2009;5:350–8.
[44] Langevin P. On the theory of Brownian motion. CR Acad Sci Paris 1908;146:530–3.
[45] Meng XY, Zhang HX, Logothetis DE, Cui M. The molecular mechanism by which PIP(2) opens the intracellular G-loop gate of a Kir3.1 channel. Biophys J 2012;102:2049–59.
[46] Meng XY, Liu S, Cui M, Zhou R, Logothetis DE. The molecular mechanism of opening the helix bundle crossing (HBC) gate of a Kir channel. Sci Rep 2016;6:29399.
[47] Hopkins CW, Le Grand S, Walker RC, Roitberg AE. Long-time-step molecular dynamics through hydrogen mass repartitioning. J Chem Theory Comput 2015;11:1864–74.
[48] Miyamoto S, Kollman PA. SETTLE: an analytical version of the SHAKE and RATTLE algorithm for rigid water models. J Comput Chem 1992;13:952–62.
[49] Ryckaert J-P, Ciccotti G, Berendsen HJC. Numerical integration of the Cartesian equations of motion of a system with constraints: molecular dynamics of n-alkanes. J Comput Phys 1977;23:327–41.
[50] Gowers RJ, Linke M, Barnoud J, Reddy TJE, Melo MN, Seyler SL, Dotson DL, Domanski J, Buchoux S, Kenney IM. Beckstein. In: Benthall S, Rostrup S, editors. Proceedings of the 15th python in science conference. 2016, 102-109, Austin, TX. SciPy; 2016.
[51] Michaud-Agrawal N, Denning EJ, Woolf TB, Beckstein O. MDAnalysis: a toolkit for the analysis of molecular dynamics simulations. J Comput Chem 2011;32:2319–27.
[52] Humphrey W, Dalke A, Schulten K. VMD: visual molecular dynamics. J Mol Graph 1996;14(33–38):27–38.
[53] Ashkenazy H, Abadi S, Martz E, Chay O, Mayrose I, Pupko T, et al. ConSurf 2016: an improved methodology to estimate and visualize evolutionary conservation in macromolecules. Nucleic Acids Res 2016;44:W344–350.
[54] Celniker G, Nimrod G, Ashkenazy H, Glaser F, Martz E, Mayrose I, et al. ConSurf: using evolutionary data to raise testable hypotheses about protein function. Isr J Chem 2013;53:199–206.
[55] Ashkenazy H, Erez E, Martz E, Pupko T, Ben-Tal N. ConSurf 2010: calculating evolutionary conservation in sequence and structure of proteins and nucleic acids. Nucleic Acids Res 2010;38:W529–533.
[56] Petit-Jacques J, Sui JL, Logothetis DE. Synergistic activation of G protein-gated inwardly rectifying potassium channels by the betagamma subunits of G proteins and Na(+) and Mg(2+) ions. J Gen Physiol 1999;114:673–84.
[57] Domene C, Klein ML, Branduardi D, Gervasio FL, Parrinello M. Conformational changes and gating at the selectivity filter of potassium channels. J Am Chem Soc 2008;130:9474–80.
[58] Pau V, Zhou Y, Ramu Y, Xu Y, Lu Z. Crystal structure of an inactivated mutant mammalian voltage-gated K(+) channel. Nat Struct Mol Biol 2017;24:857–65.
[59] Wang W, MacKinnon R. Cryo-EM structure of the open human ether-a-go-go-related K(+) channel hERG. Cell 2017;169:422–30.
[60] Dong YY, Pike AC, Mackenzie A, McClenaghan C, Aryal P, Dong L, et al. K2P channel gating mechanisms revealed by structures of TREK-2 and a complex with Prozac. Science 2015;347:1256–9.
[61] Amani R, Borcik CG, Khan NH, Versteeg DB, Yekefallah M, Do HQ, et al. Conformational changes upon gating of KirBac1.1 into an open-activated state revealed by solid-state NMR and functional assays. Proc Natl Acad Sci U S A 2020;117:2938–47.
[62] Bichet D, Grabe M, Jan YN, Jan LY. Electrostatic interactions in the channel cavity as an important determinant of potassium channel selectivity. Proc Natl Acad Sci U S A 2006;103:14355–60.